DOI: 10.1002/ ((please add manuscript number))
Article type: (**Full Paper**)

Flexible Piezoelectric Fibers for Acoustic Sensing and Positioning

*Shun Wang, Ting Zhang, Kaiwei Li, Shaoyang Ma, Ming Chen, Ping Lu and Lei Wei**

Dr. S. Wang, Dr. T. Zhang, Dr. K. Li, S. Ma, Dr. M. Chen, Prof. L. Wei
School of Electrical and Electronic Engineering, Nanyang Technological University, 50 Nanyang Avenue, 639798, Singapore
E-mail: wei.lei@ntu.edu.sg

Dr. S. Wang
Laboratory of Optical Information Technology, Wuhan Institution of Technology, Wuhan, 430205, China

Prof. P. Lu
School of Optical and Electronic Information, National Engineering Laboratory for Next Generation Internet Access System, Huazhong University of Science and Technology, Wuhan 430074, China

Prof. L. Wei
CINTRA CNRS/NTU/THALES, UMI3288, Research Techno Plaza, 50 Nanyang Drive, 637553, Singapore

Keywords: flexible electronics, piezoelectric fibers, acoustic sensors, underwater positioning

Abstract

Emerging development of flexible acoustic devices focuses on constructing large-area acoustic sensing networks with high spatial and temporal resolution, enabling the applications in acoustic sensing and positioning, particularly in underwater and medical fields. Here a piezoelectric fiber-like device is fabricated by thermal drawing technique to deliver acoustic sensing functionalities at fiber-optic length scales, flexibility and uniformity. The resulting piezoelectric fiber device operates in the frequency range of 2-8 MHz with signal-to-noise ratio above 20 dB. Additionally, a single piezoelectric fiber can simultaneously demodulate two monochromatic sound signals with the frequency gap from 0.01 MHz to 30 MHz. As a proof-of-concept, a two-dimensional 3×3 fiber array is fabricated to detect and position an underwater acoustic source with the spatial resolution of centimeter.

1. Introduction

Advances in flexible acoustic devices have enabled a broad range of studies and applications, especially in the fields that require large-area coverage of arbitrary geometry and topology for acoustic sensing or energy harvesting.[1-13] Take ocean exploitation as an example, to monitor the ocean activities, such as offshore fish farms, autonomous underwater vehicle guidance, earthquake, coastal surveillance and underwater communications, with high spatial and temporal resolution, the ideal way is to use a large-area acoustic sensing network with sufficient sensing nodes and environment-compatible mechanical flexibility.[1] Among various transducing principles of developed acoustic sensors, piezoelectric effect is the most commonly employed approach and has been adopted in underwater acoustic transducers because of its high sensitivity on converting vibration of acoustic waves to electric energy and vice versa.[14] The development of piezoelectric materials has experienced single crystals, ceramics, composites and polymers,[15] which have been used in various applications such as energy harvesters,[16] photodetectors[17,18] and capacitors.[19] Compared with conventional lead-based materials such as lead zirconate titanate (PZT) and composites with relaxor ferroelectrics, piezoelectric polymers such as polyvinylidene difluroide (PVDF) and its co-polymers poly(vinylidenefluoride-co-trifluoroethylene)[P(VDF-TrFE)] provide better acoustic impedance matching with water, higher hydrostatic response and broader bandwidth.[20] More importantly, they offer superior mechanical flexibility for the fabrication of flexible transducers in terms of both sizes and geometries, serving as a good candidate for constructing underwater acoustic sensor networks. To date however, a large number of such devices have been developed in the form of thin films, which are less favorable for aforementioned applications. On the other hand, assembling flexible piezoelectric materials and metal contacts in a well-defined geometry with microscopic cross-sectional features maintained over meter-scale lengths is fundamentally challenging. While the performance of

acoustic sensors has been continuously enhanced, a key limitation has remained unchanged: to sense or position the location of an acoustic source point with high spatial resolution, the number of zero-dimensional acoustic components acting as the sensing nodes in an acoustic sensing network must be densified, similar to the individual pixels used to create photographic images in a digital camera.

Here we present the realization of acoustic sensing in intrinsically produced, electrically connected, long and flexible fiber-like devices by utilizing the recent emergence of multi-material fibers.[21-27] This is achieved by thermal drawing technique to integrate thin layer of piezoelectric polymer P(VDF-TrFE) and metal electrodes with precisely defined interfaces. Specifically, the resulting piezoelectric fiber harnesses the unique material and mechanical properties of P(VDF-TrFE), and works as an acoustic sensor in a wide frequency range. We characterize the device performance for detecting both monochromatic acoustic wave and multiple frequencies. To position an underwater acoustic source, a two-dimensional fiber array with the grid size of 15 cm $\times$ 15 cm is constructed. Importantly, the fiber-to-fabric nature of this type of acoustic sensing array requires only a 2N number of elements to achieve N^2 detection resolution, enabling the applications related but not limited to acoustic sensing and positioning.

2. Results and discussion

To fabricate piezoelectric fibers, we rely on a method called preform-to-fiber fabrication method by constructing a macroscopic version of the desired structure and subsequently scaling it down to the microscopic dimensions via thermal drawing, as schematically shown in **Figure 1**a. P(VDF-TrFE) offers many superior properties in constructing flexible acoustic sensors, such as large piezoelectric coefficient, high mechanical flexibility, good impedance matching with water, and wide operating bandwidth.[15] More importantly, due to steric

hindrance by the bulky fluorine atoms, this copolymer assumes the ferroelectric β-phase spontaneously upon solidification from the melt without necessitating any mechanical stress, making it particularly suitable for the thermal fiber drawing process. To start, thermally pressed P(VDF-TrFE) film is sandwiched by two carbon-loaded polyethylene (CPE) layers to ensure a large active area between piezoelectric and conducting materials. Eutectic alloy bismuth-tin (BiSn) is selected as the metallic electrodes for the connection with external circuits. The entire structure is assembled between two rectangular-shaped polycarbonate (PC) blocks, and thermally consolidated to form a monolithic macroscopic preform. The preform is then thermally drawn at 230 ^{o}C, and yields tens of meters of piezoelectric fibers. Figure 1b shows the optical microscope image of the resulting piezoelectric fiber with an overall dimension of 1.6 mm×0.4 mm. The thicknesses of P(VDF-TrFE) layer and CPE layers are 10 μm and 8 μm, respectively. The metallic electrodes are continuous and well maintained in rectangular shape, and the interfaces between different materials are clearly defined as shown in the scanning electron microscopy (SEM) image of the piezoelectric fiber cross section. More images of the fiber structure can be found in Figure S1 (Supporting Information). Meanwhile, data record during the drawing fiber process and wide angle X-ray diffraction (XRD) measurement are carried out to examine the average width and composition of the as-fabricated piezoelectric fibers, respectively (Figure S2, Supporting Information). The results reveal the width ranges from 1 mm to 1.8 mm with small deviation and indicate that the drawn P(VDF-TrFE) copolymer solidifies in its β-phase with a crystallinity fraction over 90%. Owing to the almost all-polymer structure, the resulting fiber exhibits high mechanical flexibility to be easily coiled or woven. An electrical polarization necessitates the realignment of the random orientation of ferroelectric micro-domains in P(VDF-TrFE) layer to achieve macroscopic polarization (see details in Experimental Session). The good continuity and uniformity of each structural layer avoid the risk of dielectric break-down potentially induced by the very high applied electric field.

The most direct way to establish the piezoelectric response of the fiber and characterize its performance is to perform acoustic measurements, using the fabricated fibers alternately as an acoustic sensor and actuator. The measuring system is schematically shown in **Figure 2**a. Monochromatic acoustic wave from a commercial ultrasonic transducer couples to the fiber in a water tank with a fixed distance of 15 cm (about 100 acoustic wavelengths at 1 MHz). The output voltage signal of the fabricated piezoelectric fiber with length of 20 cm is collected by a digital oscilloscope after being amplified by a preamplifier. Encountering the acoustic wave with the frequency of 8 MHz driven by 10 V, Figure 2b and 2c plot the generated sinusoidal time-domain waveform and the corresponding fast Fourier transform (FFT)-resolved frequency spectrum of such a fiber with the SNR ~40 dB. We further characterize the frequency response of the piezoelectric fiber by sweeping the frequency range from 1 MHz to 13 MHz, as plotted in Figure 2d. Performing a good signal demodulation should meet the following two criteria: one is to obtain a high voltage output, i.e., in our case the average peak-to-peak voltage V_{app} should be larger than 100 mV, as the gray box indicated in Figure 2d. The other one is to achieve a detectable SNR (SNR > 20 dB in our case as the yellow box shown in Figure 2d). Therefore, the optimal working frequency range of our fiber as an acoustic sensor is from 2 MHz to 8 MHz, as the dashed red box shown in Figure 2d, which is limited by the performance of the preamplifier used in this experiment. In principle, our polymeric piezoelectric fiber could operate in a broader frequency range. In addition to working as an acoustic sensor, the piezoelectric fiber is also able to work as an actuator (Figure S3, Supporting Information). The measurement results reveal that the detected output voltage is linear to the driving voltage applied to the piezoelectric fiber and the piezoelectric fiber offers better performance in higher frequency range as an actuator.

Beyond its basic response to monochromatic acoustic wave, we further study the ability of the piezoelectric fiber to differentiate multiple frequencies by exposing it to two acoustic sources. With the same experiment settings as single source detection, **Figure 3**a and 3b plot

the waveform of output voltage and its FFT frequency spectrum with two dominant peaks when the piezoelectric fiber is under 6 MHz and 9 MHz (3 MHz frequency gap) excitation at the same time. Furthermore, the results in Figure 3c and 3d imply that our sensing device is capable to distinguish two sound waves with closer frequencies of 6 MHz and 6.01 MHz (0.01 MHz frequency gap), demonstrating an excellent detection resolution. The ability to distinguish bi-frequency sound waves covers a wide range of frequency gaps from 0.01 MHz to 30 MHz (Figure S4, Supporting Information). Since we can fully demodulate two different acoustic sources simultaneously, it is promising that three and more sound waves can also be distinguished.

The sensing performance of piezoelectric fiber mainly depends on the sound pressure variation owing to the piezoelectric effect. Simplifying the acoustic source as a vibrating particle, the sound pressure distribution in a cross section plane can be theoretically evaluated by finite element simulations as shown in **Figure 4**a. The transient distribution of underwater sound pressure follows a law of "peak-dip-peak" circular diffusion. Figure 4b gives the sound pressure attenuation lines for the transient distribution and average distribution along wave propagation direction, which exhibits a predominantly exponential dependence and corresponds to the color variation as shown in Figure 4a. Moreover, we find an interesting phenomenon by comparing the piezoelectric effects of the fiber placed parallelly (Figure 4c) and vertically (Figure 4e) to the vibrating plane. Their simulated output electric potentials are illustrated in Figure 4d and 4f, which indicate the total outputs of about 0.206 μV and 0.407 μV, respectively. The vertically positioned fiber possesses an output potential of around two times higher than that of the parallelly positioned fiber. The difference might be caused by the following two reasons: one is that the back part of the parallelly positioned fiber shields more ultrasonic pressure than that of the vertically positioned fiber due to the relatively large width. The other is that the interaction length between the transducer and the vertically positioned fiber is longer than that between the transducer and the parallelly positioned fiber.

To experimentally verify the exponential dependence of attenuation line, we characterize the underwater ultrasonic sensing performance of a single piezoelectric fiber (**Figure 5**a) and a 1×3 fiber array (Figure 5c) with their vertical direction placed to the vibrating plane (under 2 MHz and 10 V excitation). As illustrated in Figure 5b, the output root mean square voltage (Vrms) and average peak-to-peak voltage (Vapp) decrease exponentially with the respective attenuation coefficients of -0.301 and -0.286 as the distance (d) between acoustic source and fiber increases, which is consistent with the simulation results in Figure 4a and 4b. The 1×3 fiber array is set as f1′, f2′ and f3′with 10 cm intervals in L direction as represented in Figure 5c, and their distinguishable output voltage values are displayed in Figure 5d. The output value of the closest fiber f1′ (red color) is 1.50 V, which is about 0.88 times larger than that of the middle fiber f2′ (0.80 V) and 2.33 times larger than that of the farthest fiber f3′ (0.45 V). Because of the large attenuation coefficient in this situation, it is suitable for an acoustic positioning application with clear distinguishable output values. As a comparison, the situation where the fiber and vibrating plane are parallel is shown in Figure S5 (Supporting Information). Although both Vrms and Vapp also vary in an exponential dependence along d direction, their attenuation coefficients are very close (-0.147 and -0.135, respectively) and approximate twice smaller than those in Figure 5b. The measured results of a 1×3 fiber array in L direction under the same configuration show that the output value difference of the three fibers is not significant, and the output value in the closest fiber is 2.3 times as small as that in the former vertical situation (0.65 V vs 1.5 V), which is almost identical with the simulation results in Figure 4 (1.97 times). Thus, it is very difficult to distinguish which fiber is close to the source in parallelly positioned situation and unable to accomplish the acoustic positioning application. As a result, the comparison of the experimental results not only further confirms the agreement with the finite element simulation results in Figure 4, but also implies a more

applicable solution by adapting the vertically positioned configuration for underwater acoustic positioning.

Finally, we weave a flexible acoustic sensor network based on a 3×3 piezoelectric fiber array as a prototype to demonstrate the two-dimensional underwater acoustic positioning application (Figure 5e). The 3×3 acoustic sensor array with the grid size of 15 cm × 15 cm is constructed by 6 piezoelectric fibers as the insert image shown in Figure 5e. By analyzing all the voltage outputs of the 6 fibers (V_{f1}, V_{f2}, V_{f3}, $V_{f1'}$, $V_{f2'}$, and $V_{f3'}$), two distinguishable signals from each grid axis can infer the accurate position of an underwater ultrasonic source. For example, in the case shown in Figure 5e, the position of the acoustic source is resolved under the cross point of f1 and f2' as indicated by a red star. Furthermore, the accurate depth from the source to the cross point is determined by the two largest output voltage values according to the attenuation line measured before. These results suggest that the specific underwater acoustic positioning is achieved, and large-area acoustic sensor network based on piezoelectric fiber array has the great potential to identify and map underwater acoustic profiles.

It is worth noting that the acoustic sensor networks with different fiber numbers and the same grid size will not influence the sensing performance but just change the sensing scale. According to the experimentally measured attenuation lines as shown in Figure 5b, we can find the performance of acoustic sensor network is mainly up to its grid size which affects the distances between the ultrasonic source and the fibers. To make it more clearly, we also experimentally present the sensing performances of the acoustic sensor networks with different grid sizes (3 cm × 3 cm and 20 cm × 20 cm in a 3×3 array) in Figure S6 (Supporting Information). The results demonstrate that the acoustic sensor network with smaller grid size is difficult to position an acoustic source due to the similar voltage outputs, while the network

with the larger grid size can localize an acoustic source more easily owing to the large differences of the voltage outputs on each intersection.

While the frequency gap in our experiment is not so narrow like some recently reported results (the nearest 0.01 MHz vs 0.05 Hz),[4] our working frequency range (~MHz) is much higher than that demonstrated before (~100 Hz), which leads to the possibility to further reduce the frequency gap between different sound waves at lower working frequency range. Further improvement in process development and material quality is expected to achieve better device performance. First, composite polymer formed by introducing some nanoparticles with strong piezoelectric coefficients such as PZT in P(VDF-TrFE) will significantly improve the piezoelectric properties and maintain good flexibility of the resulting piezoelectric fibers. Second, increasing the thickness or the number of layers of piezoelectric material will greatly improve the acoustic sensitivity of our piezoelectric fiber sensor. In fact, the proposed fabrication process is highly versatile, allowing a variety of families of functional materials that are sensitive to other physical parameters to be integrated in a single fiber, for example, an energy-harvesting fiber could be realized with the integration of organic thermoelectric polymers, such as polyaniline,[28] polythiophene[29] and especially for poly(3,4-ethylenedioxythiophene)(PEDOT):poly(4-styrenesulfonic acid)(PSS). [30, 31]

Furthermore, the fiber shape, rectangular cross-section in our article, can be designed as other shapes such as circular or triangular when used in different places.[22] Besides the improvable sensing performance and versatile functionalities of the single piezoelectric fiber, the geometry topology of our sensing networks is also various. Actually not only 2D array but also sophisticated 3D array of sensing networks can be achieved based on different application demands and fields.[21] In another word, both the fiber shape and geometry topology of our sensing networks are flexible and can be further customized.

3. Conclusions

In summary, a flexible polymeric acoustic sensor is fabricated by thermally co-drawing multiple disparate materials into a piezoelectric fiber. The resulting piezoelectric fiber is capable to efficiently detect underwater acoustic source in the frequency range from 2 to 8 MHz with SNR above 20 dB and demodulate multiple frequencies simultaneously. Both theoretical and experimental results suggest that the fiber with vertical direction can achieve stronger output voltage than that of the fiber with parallel direction. Furthermore, a flexible acoustic sensor network by 3×3 piezoelectric fiber arrays is also experimentally applied for underwater positioning application. The interplay between materials properties and structure integration in these fibers opens up opportunities to deliver novel device functionalities at fiber-optic length scales, flexibility, and uniformity, leading to the realization of more sophisticated functionalities and the prospect of truly multifunctional fibers.

4. Experimental Section

Fabrication of flexible piezoelectric fibers: The processes begin with milling to assemble the layers with different materials, including piezoelectric material P(VDF-TrFE), electrode material CPE and BiSn wires, and cladding material PC. Then the assembled structure is consolidated in a vacuum oven at 185℃ for 20 minutes to remove the trapped gas and form high quality interfaces. The resulting preform is then thermally drawn to tens of meters of piezoelectric fiber in a vertical tube furnace with three hot zones temperature of 150 ℃, 230 ℃ and 110 ℃, respectively.

Polarize the piezoelectric fiber: The resulting piezoelectric fiber is polarized in strong external electric field to express piezoelectricity. The polarization procedure is described as follows. Firstly, electric contacts are made by stripping away the PC cladding layer to expose the built-in BiSn electrodes using a microtome blade under a stereomicroscope. Then copper

wires are wrapped around the exposed electrodes and firmly fixed with conductive silver paint. Last, strong external electric field (60 MV/m) is applied to the contacted piezoelectric fiber samples for 10 minutes for polarization.

Characterization: The morphologies of samples are examined by a scanning electron microscope (Phenom Pro SEM) and Digital Microscopy (Olympus BX51). A commercial ultrasonic transducer (Olympus Panametrics-NDT, 1.0 MHz-centered) links to waveform generator (Agilent 33250A, Maximum 80 MHz) to generate monochromatic sounds. The output voltage signal of our piezoelectric fiber is displayed in the digital oscilloscope (LecROY WaveSurfer 104MXs-B, 1 GHz bandwidth) after being amplified by the preamplifier (Olympus preamplifier 5662, 34 dB).

Finite element simulation: Using COMSOL Multiphysics software to study the sound pressure distribution of acoustic source during the underwater propagation, the ultrasonic source here is simply served as a vibrating particle with a radius of 1 mm. The total radius of acoustic domain underwater is 5 mm including 1 mm viscous boundary layer. The parameter of underwater sound velocity is 1500 m/s and ultrasonic frequency is 2 MHz. Besides, in order to compare the performance of acoustic fiber sensor under different working mechanisms, the fiber piezoelectric layers are considered as electroacoustic membrane transducers with two different sizes. One is 2 mm radius and 80 μm thickness (Figure 4c), while the other is 0.35 mm radius and 1.3 mm thickness (Figure 4e). Material parameters are chosen to be close to the actual situation, namely, P(VDF-TrFE) with density of 1800 kg/m^3, elastic modulus of 2.5 GPa and Poisson's ratio of 0.4. Other parameters are set as follows. Membrane static tension is 3150 N/m, external incident pressure is 1 Pa, and bulk viscosity is 10^{-6} Pa·s. Furthermore, the upper surface of the piezoelectric layer is set as the ground, and then the electric potential of the whole layer can be monitored and analysed.

Supporting Information

Supporting Information is available from the Wiley Online Library or from the author.

Acknowledgements

S. Wang and T. Zhang contributed equally to this work. This work is supported in part by the Singapore Ministry of Education Academic Research Fund Tier 2 (MOE2015-T2-1-066, MOE2015-T2-2-010), and Nanyang Technological University (Start-up grant: Lei Wei).

Received: ((will be filled in by the editorial staff))
Revised: ((will be filled in by the editorial staff))
Published online: ((will be filled in by the editorial staff))

References

[1] B. E. Eovino, M.S. *Thesis*, University of California, Berkeley, USA **2015**.

[2] Z. Liu, X. Zhang, Y. Mao, Y. Y. Zhu, Z. Yang, C. T. Chan, P. Sheng, *Science* **2000**, 289, 1734.

[3] K. Song, S. H. Lee, K. Kim, S. Hur, J. Kim, *Sci. Rep.* **2014**, 4, 4165.

[4] C. Lang, J. Fang, H. Shao, X. Ding, T. Lin, *Nat. Commun.* **2016**, 7, 11108.

[5] G. Papadakis, A. Tsortos, A. Kordas, I. Tiniakou, E. Morou, J. Vontas, D. Kardassis, E. Gizeli, *Sci. Rep.* **2013**, 3, 2033.

[6] G. Papadakis, A. Tsortos, E. Gizeli, *Nano Lett.* **2010**, 10, 5093.

[7] G. Ma, M. Yang, S. Xiao, Z. Yang, P. Sheng, *Nat. Mater.* **201**4, 13, 873

[8] S. N. Cha, J. S. Seo, S. M. Kim, H. J. Kim, Y. J. Park, S. W. Kim, J. M. Kim, *Adv. Mater.* **2010**, 22, 4726.

[9] S. Viola, M. Ardid, V. Bertin, A. Enzenhofer, P. Keller, R. Lahmann, G. Larosa, C. D. Llorens, *Nucl. Instrum. Meth. A* **2013**, 725, 207.

[10] N. Chocat, G. Lestoquoy, Z. Wang, D. M. Rodgers, J. D. Joannopoulos, Y. Fink, *Adv. Mater.* **2012**, 24, 5327.

[11] H. Jin, J. Zhou, X. He, W. Wang, H. Guo, S. Dong, D. Wang, Y. Xu, J. Geng, J.K. Luo, W. I. Milne, *Sci. Rep.* **2013**, 3, 2140.

[12] J. Luo, X. He, J. Zhou, W. Wang, W. Xuan, J. Chen, H. Jin, Y. Xu, S. Dong, *Procedia Eng.* **2015**, 120, 717.

[13] M. B. Dentry, J. R. Friend, L. Y. Yeo, *Lab Chip* **2014**, 14, 750.

[14] C. H. Sherman, J. L. Butler, *Transducers and arrays for underwater sound*, Springer, New York, NY, USA **2007**.

[15] H. Li, Z. D. Deng, T. J. Carlson, *Sensor Lett.* **2012**, 10, 679.

[16] M. Lee, C.Y. Chen, S. Wang, S.N. Cha, Y. J. Park, J. M. Kim, L. J. Chou, Z. L. Wang, *Adv. Mater.* **2012**, 24, 1759.

[17] L. Peng, L. Hu, X. Fang, *Adv. Funct. Mater.* **2014**, 24, 2591.

[18] H. Chen, H. Liu, Z. Zhang, K. Hu, X. Fang, *Adv. Mater.* **2016**, 28, 403.

[19] P. Skládal, *TrAC Trends Anal. Chem.* **2016**, 79, 127-133.

[20] D. K. Kharat, S. Mitra, S. Akhtar, V. Kumar, *Defence Sci. J.* **2007**, 57, 7.

[21] A. F. Abouraddy, M. Bayindir, G. Benoit, S. D. Hart, K. Kuriki, N. Orf, O. Sharira, F. Sorin, B. Temelkuran, Y. Fink, *Nat. Mater.* **2007**, 6, 336.

[22] S. Egusa, Z. Wang, N. Chocat, Z. M. Ruff, A. M. Stolyarov, D. Shemuly, F. Sorin, P. T. Rakich, J. D. Joannopoulo, Y. Fink, *Nat. Mater.* **2010**, 9, 643.

[23] A. M. Stolyarov, L. Wei, O. Shapira, F. Sorin, S. L. Chua, J. D. Joannopoulos, Y. Fink, *Nat. Photonics* **2012**, 6, 229.

[24] A. Gumennik, L. Wei, G. Lestoquoy, A. M. Stolyarov, X. Jia, P. H. Rekemeyer, M. J. Smith, X. Liang, B. Grena, S. G. Johnson, S. Gradečak, A. F. Abouraddy, J. D. Joannopoulos, Y. Fink, *Nat. Commun.* **2013**, 4, 2216.

[25] C. Hou, X. Jia, L. Wei, A. M. Stolyarov, O. Shapira, J. D. Joannopoulos, Y. Fink, *Nano Lett.* **2013**, 13, 975.

[26] A. Canales, X. Jia, U. Froriep, R. Koppes, C. Tringides, J. Selvidge, C. Lu, C. Hou, L. Wei, Y. Fink, P. Anikeeva, *Nat. Biotechnol.* **2015**, 33, 277.

[27] C. Hou, X. Jia, L. Wei, S. Tan, X. Zhao, J. Joannopoulos, Y. Fink, *Nat. Commun.* **2015**, 6, 6248.

[28] Q. Yao, L. Chen, W. Zhang, S. Liufu, X. Chen, *ACS Nano* **2010**, 4, 2445.

[29] M. He, J. Ge, Z. Lin, X. Feng, X. Wang, H. Lu, Y. Yang, F. Qiu, *Energy Environ. Sci.* **2012**, 5, 8351.

[30] G. Kim, L. Shao, K. Zhang, K. P. Pipe, *Nat. Mater.* **2013**, 12, 719.

[31] O. Bubnova, Z. U. Khan, A. Malti, S. Braun, M. Fahlman, M. Berggren, X. Crispin, *Nat. Mater.* **2011**, 10, 429.

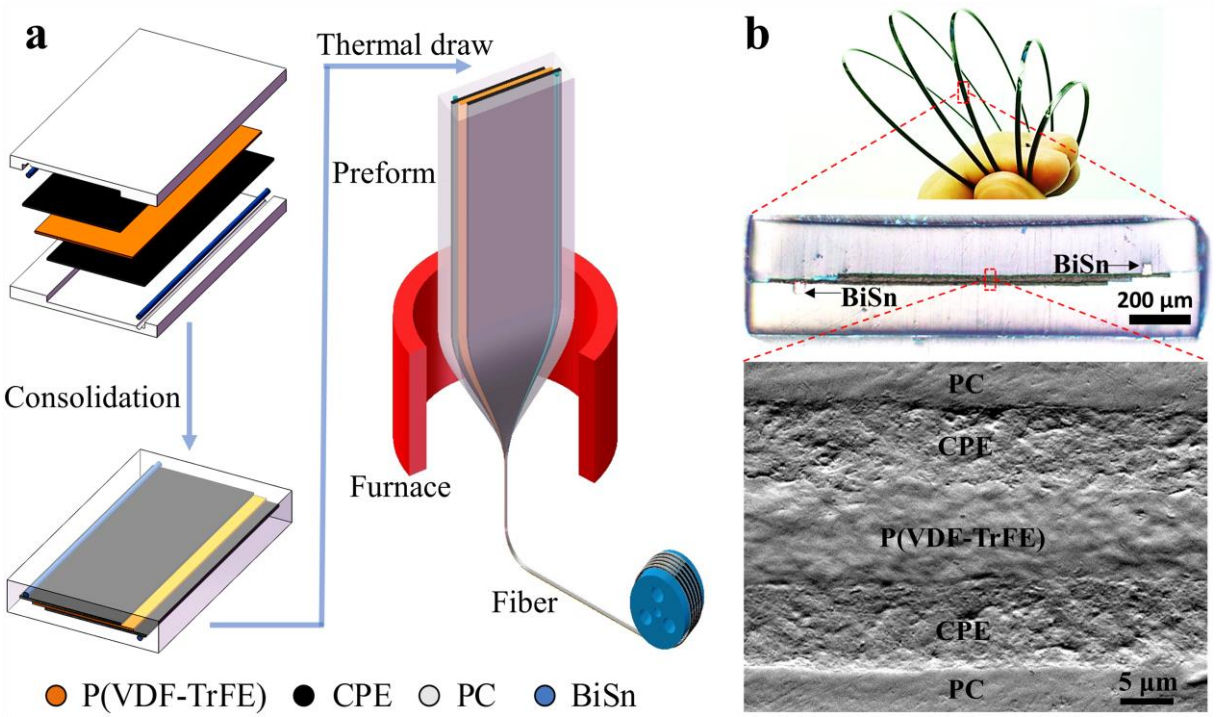

Figure 1. Fabrication of piezoelectric fibers. (a) Schematic diagram of the fabrication process of a piezoelectric fiber. (b) Digital photo, optical microscope image and the cross-section SEM image of the fabricated piezoelectric fiber.

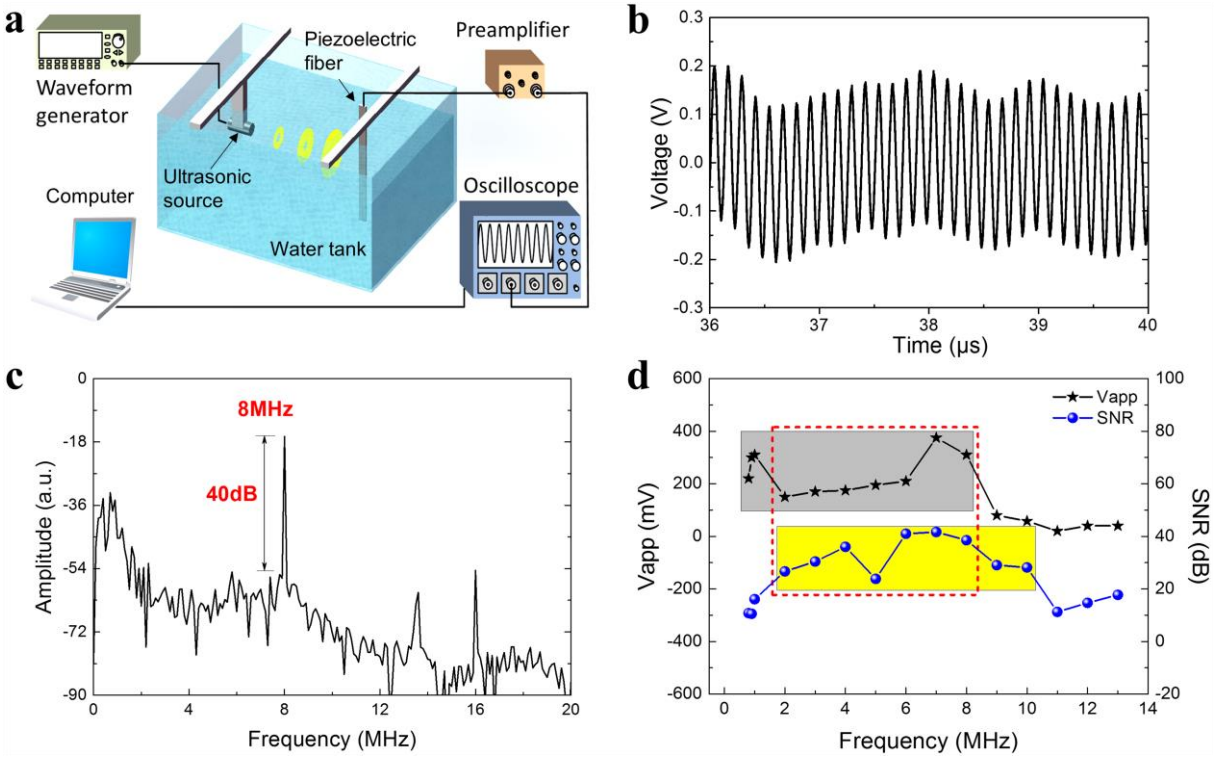

Figure 2. Acoustic sensing performance of a piezoelectric fiber. (a) Schematic setup for testing the performance of an acoustic fiber sensor. (b) Voltage outputs of the piezoelectric fiber device at 8 MHz and (c) its FFT-processed frequency spectrum. (d) Frequency response of the acoustic fiber sensor. The gray box indicates the frequency range in which the average peak-to-peak voltage V_{app} is larger than 100 mV, while the yellow box plots the frequency range in which a detectable SNR (SNR > 20 dB in our case) is achieved. Therefore, the optimal working frequency range of the fabricated piezoelectric fiber as an acoustic sensor is from 2 MHz to 8 MHz, as marked by the dashed red box.

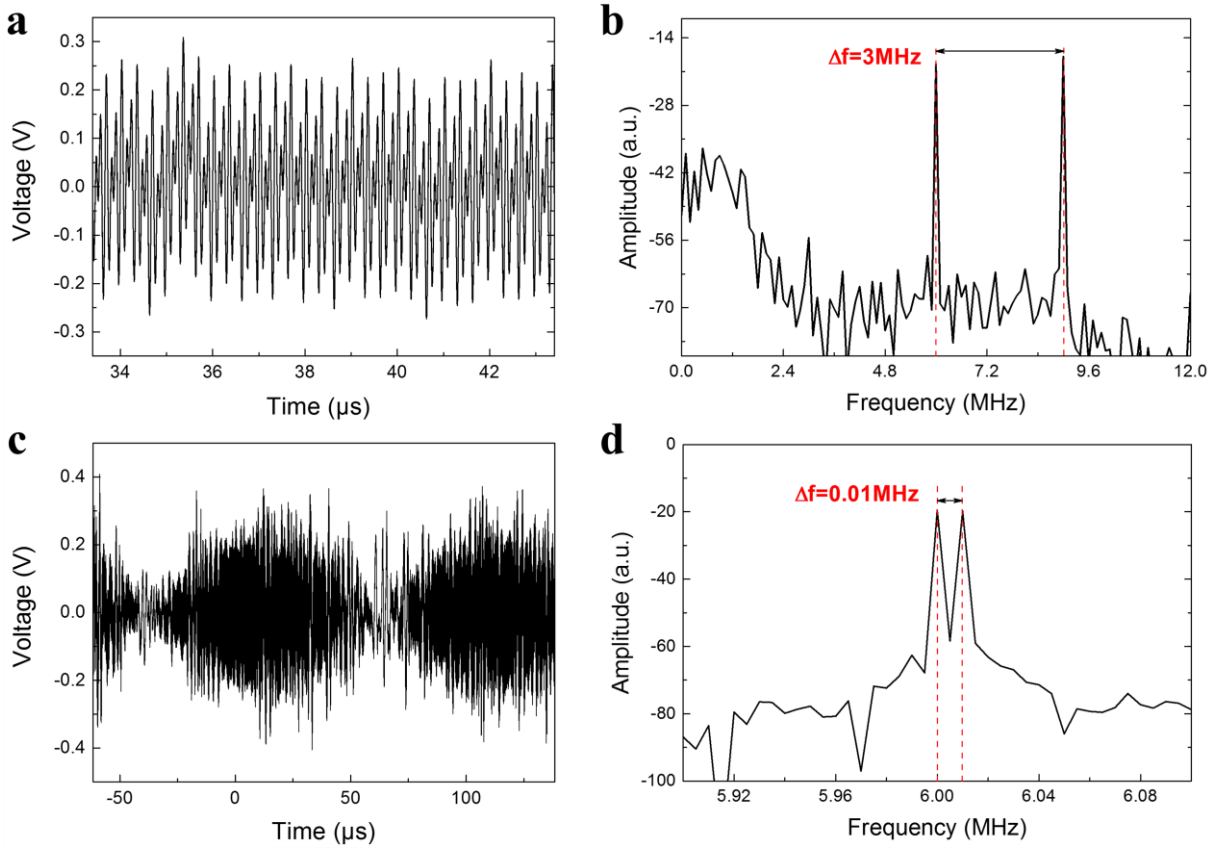

Figure 3. Voltage outputs of the piezoelectric fiber for detecting two monochromatic sound waves simultaneously and the FFT-processed frequency spectra. (a) Voltage outputs under 6 MHz and 9 MHz at the same time with the frequency spectrum in (b). (c) Voltage outputs of 6 MHz and 6.01 MHz with the frequency spectrum in (d).

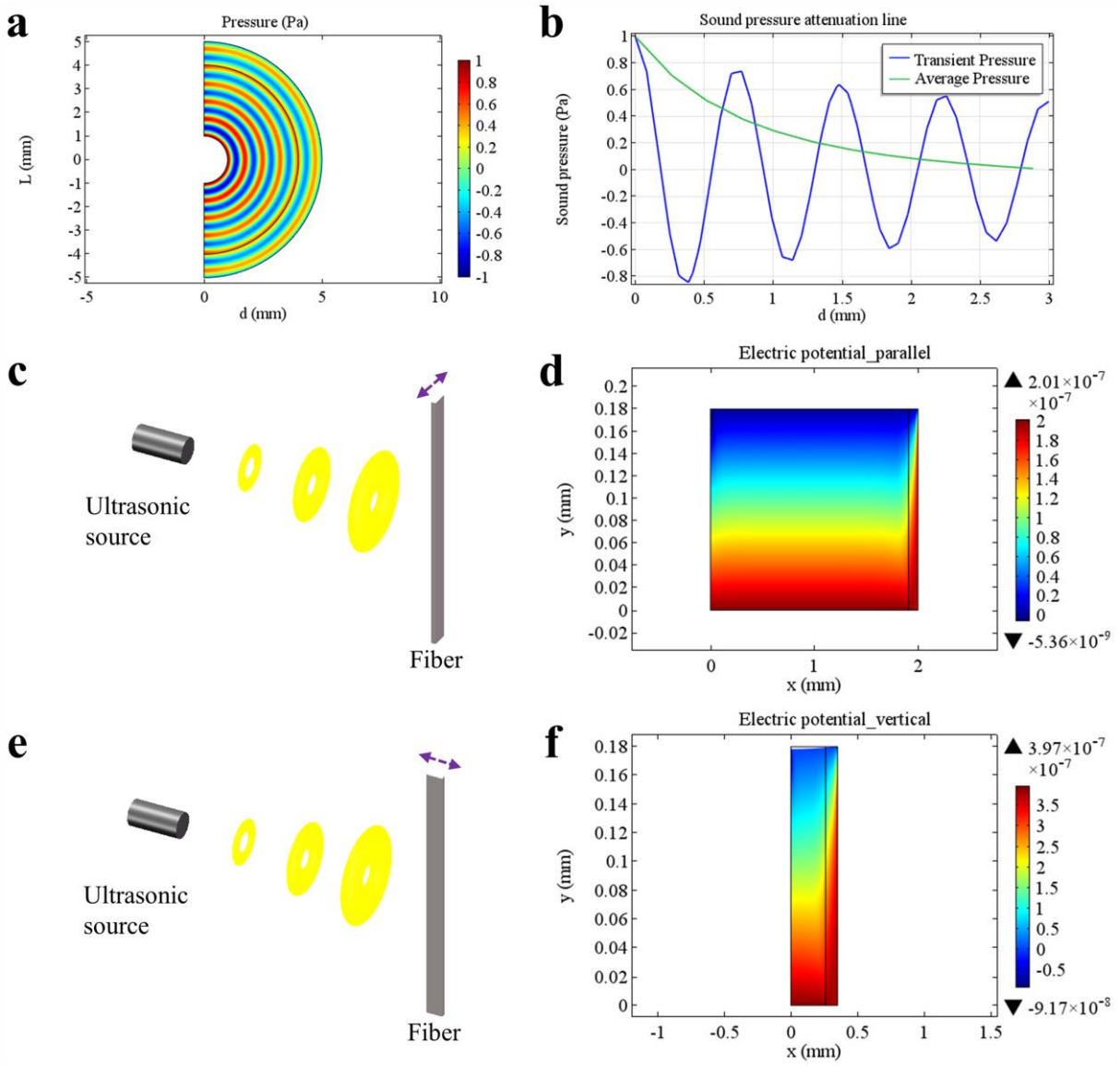

Figure 4. Finite element simulation of the acoustic pressure distribution of a vibration acoustic source and the performance comparison of piezoelectric fibers under different positioned configurations. (a) Sound pressure distribution in a cross section plane. (b) The transient pressure change and the average pressure attenuation along wave propagation direction. (c) Diagrammatic sketch of the acoustic fiber sensor for a positioned configuration that the fiber direction (as the purple arrow shows) is parallel to the sound wave vibrating plane, and its simulated output electric potential in (d). (e) The other positioned configuration that the fiber direction is vertical to the sound wave vibrating plane and its simulation output result of electric potential in (f).

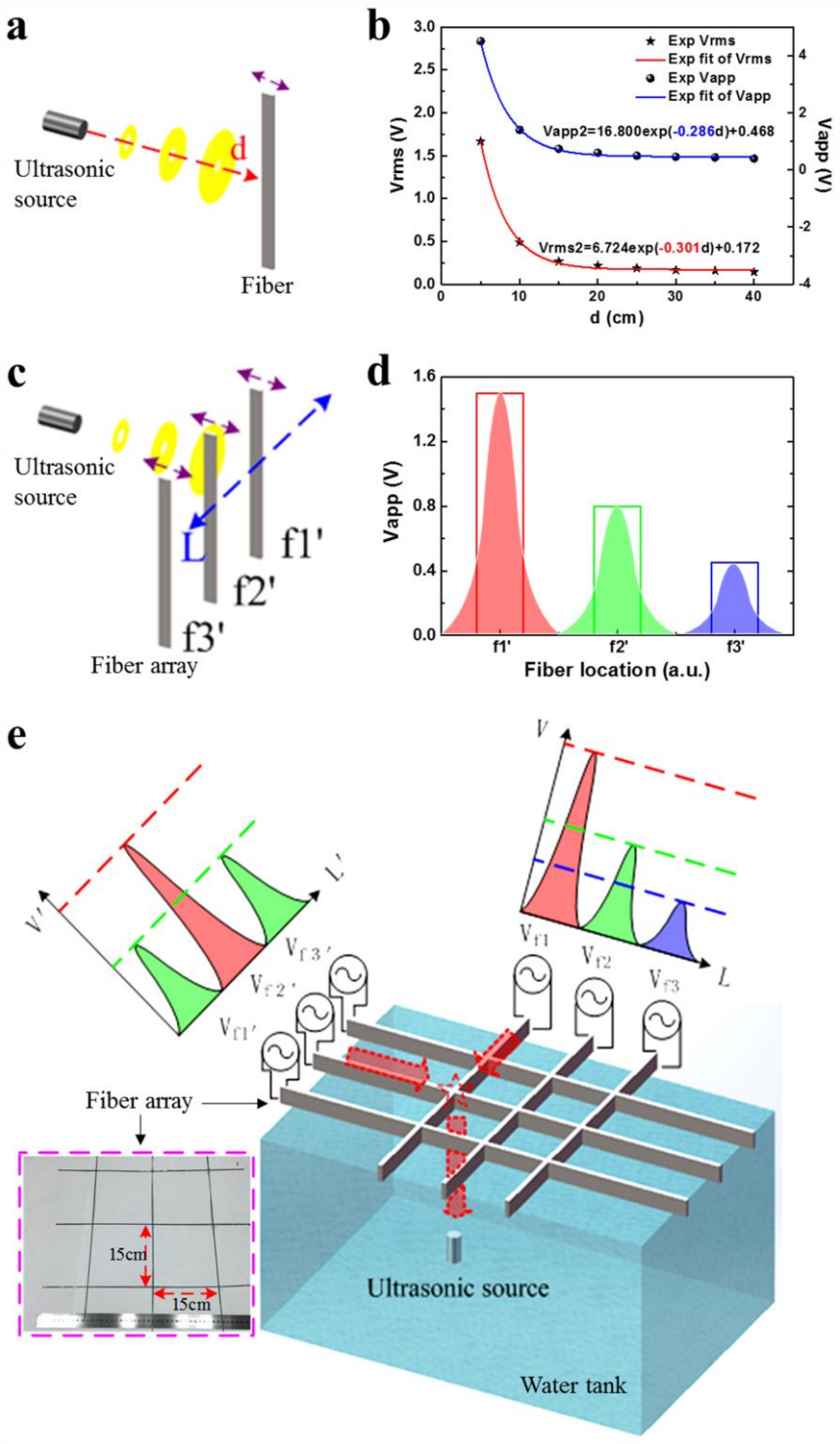

Figure 5. Acoustic sensor performance of single piezoelectric fiber, 1×3 array and 3×3 array with the fiber placed vertically to the vibrating plane for underwater acoustic source detection and positioning. (a) Diagrammatic sketch of single underwater ultrasonic fiber sensor and its attenuation results with the increased distance between acoustic source and fiber in (b). (c) Piezoelectric fibers based 1×3 acoustic sensor array and its corresponding measured results in (d). Here f1', f2' and f3' represent the three piezoelectric fibers. (e) Schematic of an acoustic sensor network based on a 3×3 piezoelectric fiber array for underwater acoustic positioning. The accurate underwater position of an ultrasonic source can be located by analyzing voltage outputs of the 6 fibers (V_{f1}, V_{f2}, V_{f3}, $V_{f1'}$, $V_{f2'}$, and $V_{f3'}$). The insert in the red dashed box is the image of the resulting3×3 piezoelectric fiber array with the grid size of 15 cm × 15 cm.